International Journal of Microwave and Wireless Technologies

cambridge.org/mrf

A single-layer band-stop frequency selective surface with wide angular stability property

Hang Gu[1], Wei Zhao[1], Fan Zhang[2] and Chao Yang[3]

[1]Key Laboratory of Electronic Equipment Structure Design, Ministry of Education, Xidian University, Xi'an, China; [2]Science and Technology on Antenna and Microwave Laboratory, Xidian University, Xi'an, China and [3]School of Science, Xi'an University of Posts and Telecommunications, Xi'an, China

Research Paper

Cite this article: Gu H, Zhao W, Zhang F, Yang C (2024) A single-layer band-stop frequency selective surface with wide angular stability property. *International Journal of Microwave and Wireless Technologies* **16**(2), 260–267. https://doi.org/10.1017/S1759078723001599

Received: 20 December 2022
Revised: 4 December 2023
Accepted: 11 December 2023

Keywords:
angular stability; frequency selective surface (FSS); miniaturization; polarization insensitivity

Corresponding author: Wei Zhao;
Email: weizhao@xidian.edu.cn

Abstract

In this paper, a single-layer band-stop frequency selective surface (FSS) by combination of Mike Kastle unit and square ring unit is proposed to achieve wide angular stable shielding. Owing to the rotational symmetry of the structure, the designed FSS is insensitive to polarization. By the combination design, the wide angular stability can be achieved as the incident angle increases from 0° to 85°, with only a maximum frequency deviation of 0.012 GHz. Meanwhile, the mechanism of the proposed FSS is investigated by the parametric analysis of equivalent circuit model. The prototype was manufactured and measured to verify the design and simulation analysis, and the measurement results were in good agreement with the simulation results.

Introduction

Frequency selective surface (FSS), an artificial periodic array of metal patches [1–4], has been widely used in the various fields of microwave engineering such as electromagnetic interference shielding, absorber, and radome [5–9]. As one of the most important properties, the angular stability is crucial for the performance of FSS and is thus required to be specially considered in the design procedure. Under the excitation condition of the incident electromagnetic wave with different angles and polarizations, the output response of FSS changes in a difficultly predictable way. In this condition, if the response is unstable under different excitations, the FSS suffers degraded performance and even loses the expected function. Therefore, designing the FSS with the wide angular stability property becomes a topic of great interest to researchers.

The miniaturization is most frequently adopted to enhance the angular stability of FSS. Under this background, much work has been made to realize 2D structures with miniaturization [10–13]. In a study by Natarajan et al. [10], an FSS with a modified swastika structure is proposed and applied to 5G shielding, which can achieve angular stabilization up to 60° with a miniaturization of $0.117\lambda_0$. Ghosh and Srivastava [11] present an FSS structure capable of achieving up to 75° angular stabilization with a miniaturization level of $0.065\lambda_0$. In the presented structure, two meander strips are designed to obtain the dual-band characteristic and independent polarization. In a study by Zhao et al. [12], the designed FSS consists of a swastika structure and four identical second iterations of H-shaped fractal parts. This design features the angular stability up to 80° and the polarization insensitivity due to the rotational symmetry. A single-layer band-stop FSS loaded with lumped elements is investigated in [13], which provides high inductance and capacitance values in the unit plane. By this means, a high level of miniaturization can be obtained, but the manufacturing cost is relatively expensive. At the same time, as the manufacturing technology gets mature, 2.5D/3D structures of FSS have gained more and more concerns [14–16]. The bandpass 2.5D FSS structure proposed in a study by Zhao et al. [14] is composed of a folded swastika slot and a vertical metal vias, which can implement the independent polarization and the angular stabilization up to 75°. Abidin et al. [15]. design a band-stop FSS to achieve a wide bandwidth of 1–4.5 GHz around the operating frequency of 2.4 GHz. This design links the upper and lower layers of metal patches through metal vias, enabling it to acquire the unit size of $0.04\lambda_0$ and guarantee the angular stability up to 75°. In a study by Li et al. [16], a 3D FSS structure based on hybrid slotted and microstrip lines makes full use of the vertical space, so that the unit cycle size is reduced and the angular stability is satisfied from 0° to 60°.

In comparison to 2D structures, 2.5D/3D structures are more suitable to achieve sharp filter response and high angular stability due to the utilization of vertical space. However, 2.5/3D structures are relatively of thick size, so that they are less applicable in many certain scenarios. In addition, it is not easy to realize 2.5D/3D structures due to the relative complexity of fabrication. By contrast, as the simplest 2D structure, the single-layer FSS has the advantage that it is more convenient to analyze, machine, and apply. Therefore, the single-layer FSS with the wide angular stability property is always the most valuable option.

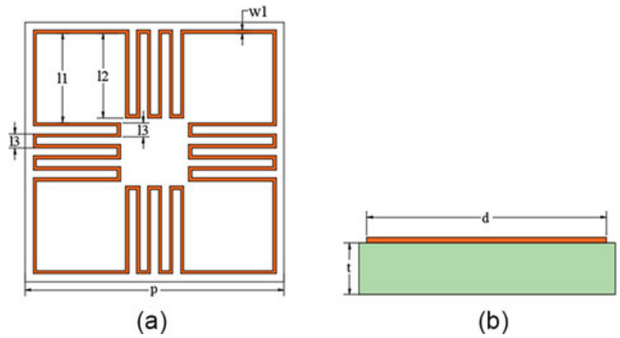

Figure 1. Structure of the designed FSS unit: (a) top view and (b) side view. FSS = frequency selective surface.

Table 1. FSS structural parameters (mm)

*l*1	*l*2	*l*3	*w*1	*p*	*d*	*t*
2.75	2.6	0.44	0.1	8	7.5	1

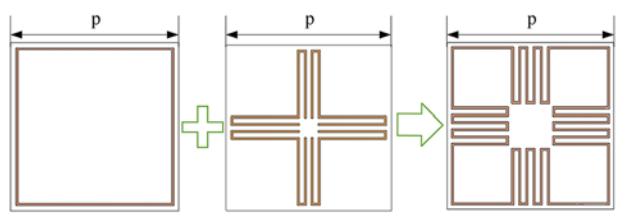

Figure 2. Component units of the designed FSS. FSS = frequency selective surface.

In this paper, a single-layer band-stop FSS with wide angular stability is proposed by integrating the square-loop unit with Mike Kastle (MK) unit. During the design process, the frequency response of the proposed FSS structure is simulated with the commercial software CST DESIGN ENVIRONMENT. Meanwhile, the equivalent circuit model (ECM) is established and used to describe the behavior of the FSS. Then, by combining the simulated results from both CST and ECM, the characteristic parameters of FSS are analyzed and optimized. Through the iterative design, the angular stability can be achieved up to 85° in both the transverse electric (TE) and the transverse magnetic (TM) polarization modes. Finally, after fabrication and measurement, the performance of the designed FSS is verified. In addition, by comparison with some other recent work, the superiority of the designed FSS is also illustrated. Therefore, the structure proposed in this work can be effectively used to shield sub-6G signals and serve as a reference unit for subsequent research on angular stability structures.

Theory

Figure 1 shows the structure of the FSS unit designed in this work. The orange and green parts represent the metal patch and the dielectric substrate, respectively. The material of the dielectric substrate is F4BK300, with a relative dielectric constant of 3 and a loss angle tangent of 0.001. The specific structural parameters of this FSS unit are given in Table 1.

Structural design and simulation

As shown in Fig. 2, the FSS unit structure integrates a square ring unit with an MK unit. As the incident angle changes from 0° to 85°, the transmission coefficients of square ring unit and MK unit are simulated by CST. Figure 3 shows that the square ring unit works at a resonant frequency of 6.34 GHz with a maximum deviation of 0.34 GHz (5.36%). Also, it can be observed from Fig. 4 that the resonant frequency of the MK unit is 10 GHz and the maximum deviation of the resonant frequency is 0.14 GHz (1.4%).

The angle stable properties of both the square ring unit and the MK unit are obvious from Figs. 3 and 4, so this work combines them together to further enhance the angular stability and the miniaturization. As shown in Fig. 5, when the incident angle changes from 0° to 85°, the resonant frequency of the proposed FSS remains 3.76 GHz with a maximum deviation of 0.012 GHz (0.32%). It can be seen that under the TE polarization, the bandwidth of |S21| increases with the incident wave angle θ, while under the TM polarization, the bandwidth of |S21| decreases with θ. This is because the characteristic impedances of TE and TM are, respectively, defined as $Z_0/\cos(\theta)$ and $Z_0\cos(\theta)$, which suggests the opposite bandwidth trends of TE and TM with the angle θ [17]. From Table 2, it is summarized that the designed FSS has the best miniaturization and the smallest deviation with the incident angle from 0° to 85°.

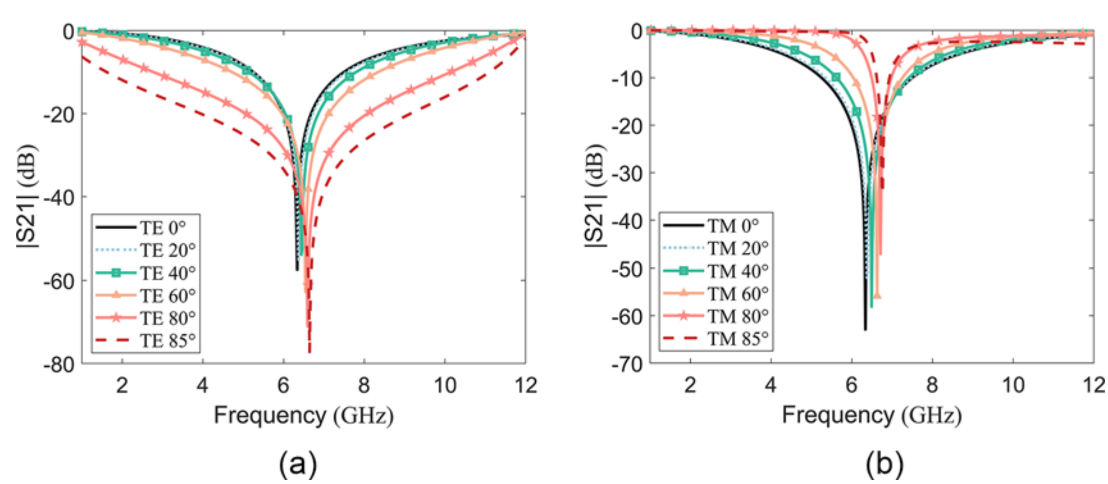

Figure 3. Transmission coefficient of the square ring unit. (a) TE polarization. (b) TM polarization.

https://doi.org/10.1017/S1759078723001599 Published online by Cambridge University Press

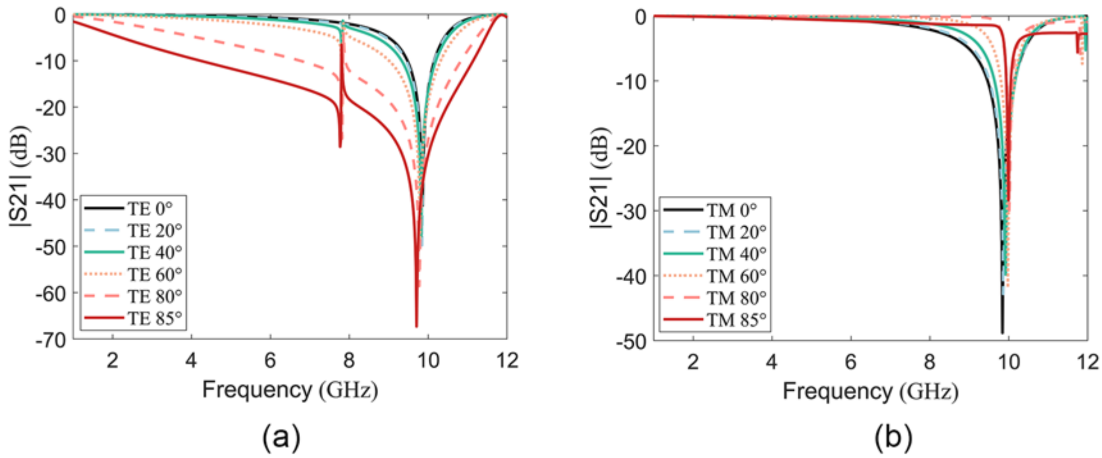

Figure 4. Transmission coefficient of the MK unit. (a) TE polarization. (b) TM polarization.

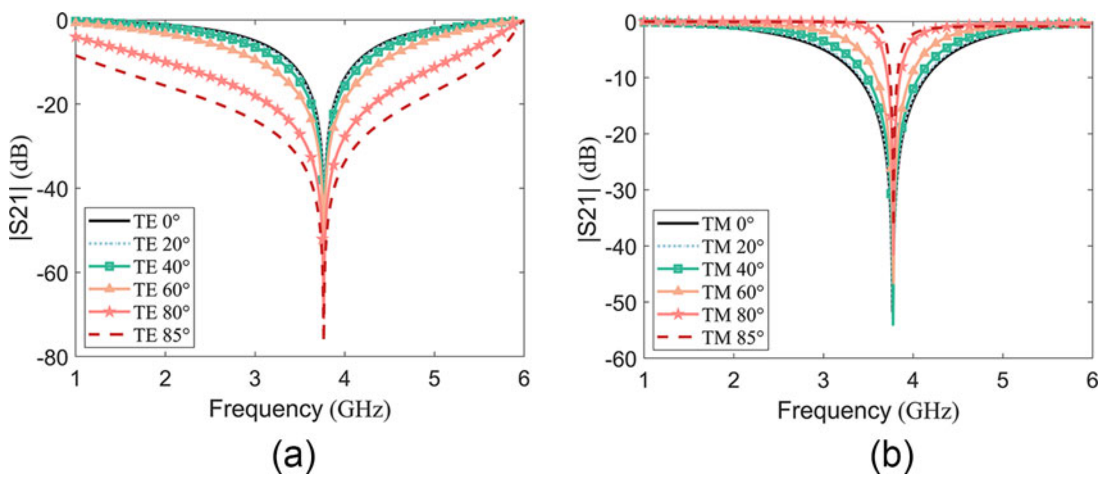

Figure 5. Transmission coefficient of the designed FSS unit. (a) TE polarization. (b) TM polarization. FSS = frequency selective surface.

Table 2. Comparison of the three different units

Unit type	Unit size (mm)	Miniaturization	Deviation (GHz)
Square ring unit	8	$0.169\lambda_0$	0.34
MK unit	8	$0.26\lambda_0$	0.14
Designed FSS unit	8	$0.1\lambda_0$	0.012

ECM analysis

From Fig. 6, it can be seen that the inductance L1 and the capacitance C1 correspond to the strip of unit and the gap between units, respectively. In addition, the capacitance C2 is introduced to represent the electric field at the center of the unit. In the case of normal incidence, the values of the lumped elements can be approximated by referring to the analysis and derivation in [18, 19] as follows:

$$L1 = \frac{Z_0 l}{\omega p} F\left(p, s, \lambda\right) \tag{1}$$

$$C1 = 4\frac{Y_0 d_1}{\omega p} F\left(p, g_1, \lambda\right) \varepsilon_{eff} \tag{2}$$

$$C2 = 4\frac{Y_0 d_2}{\omega p} F\left(p, g_2, \lambda\right) \varepsilon_{eff} \tag{3}$$

where

$$\begin{cases} l = d + 6 \times l2 \\ d_1 = 2 \times l1 + 2 \times l3 + 4 \times w1 \\ d_2 = 3 \times l3 \\ s \approx 2 \times w1 \\ g_1 = p - d \\ g_2 = d - 2 \times l2 - 2 \times w1 \end{cases} \tag{4}$$

$$F\left(p, w, \lambda\right) = \frac{p}{\lambda}\left[\ln\left(\csc\frac{\pi w}{2p}\right) + G\left(p, w, \lambda\right)\right] \tag{5}$$

$$G\left(p, w, \lambda\right) = \frac{0.5(1-\beta^2)^2\left[2A\left(1-\frac{\beta^2}{4}\right) + 4\beta^2 A^2\right]}{\left(1-\frac{\beta^2}{4}\right) + 2A\beta^2\left(1+\frac{\beta^2}{2}-\frac{\beta^4}{4}\right) + 2\beta^6 A^2} \tag{6}$$

$$A = \frac{1}{\sqrt{1-\left(\frac{p}{\lambda}\right)^2}} - 1 \tag{7}$$

$$\beta = \sin\left(\frac{\pi w}{2p}\right). \tag{8}$$

https://doi.org/10.1017/S1759078723001599 Published online by Cambridge University Press

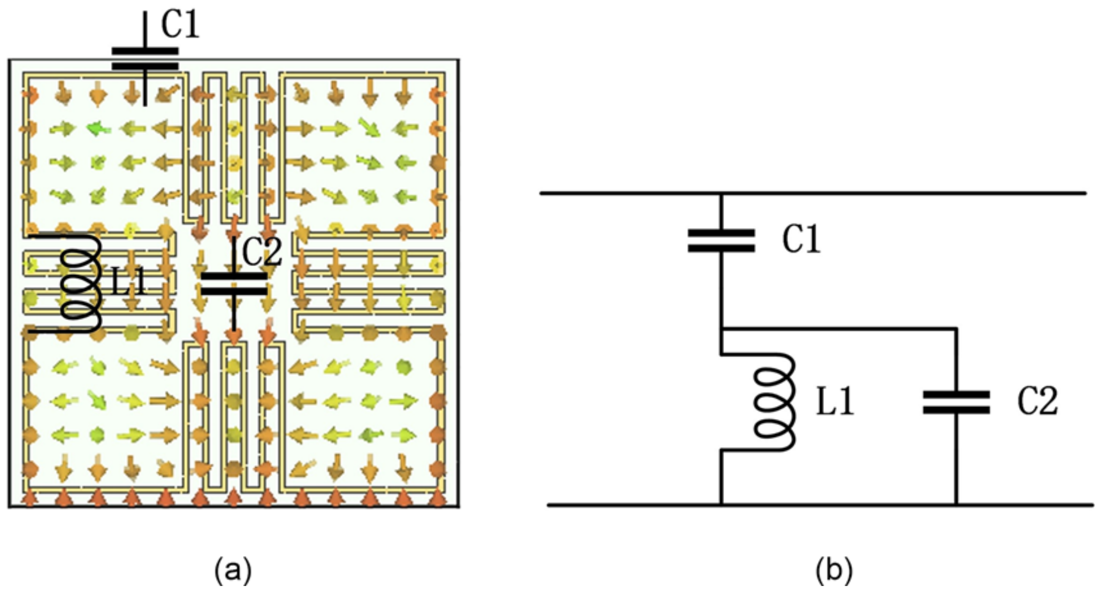

Figure 6. Field-circuit analysis of the designed FSS unit. (a) E-filed distribution. (b) Lumped-element circuit. FSS = frequency selective surface.

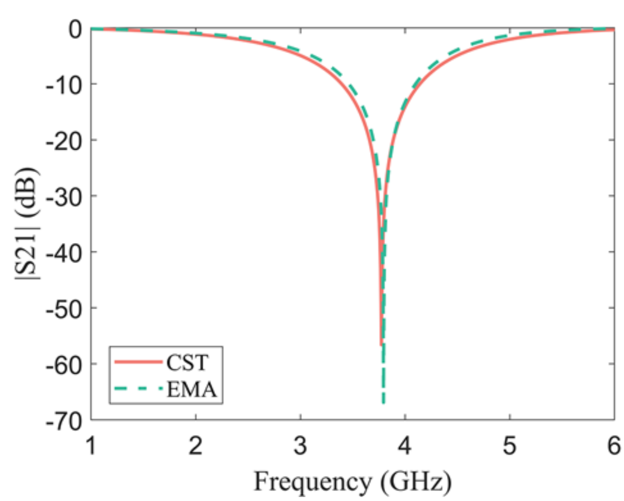

Figure 7. Comparison between ECM and CST. ECM = equivalent circuit model.

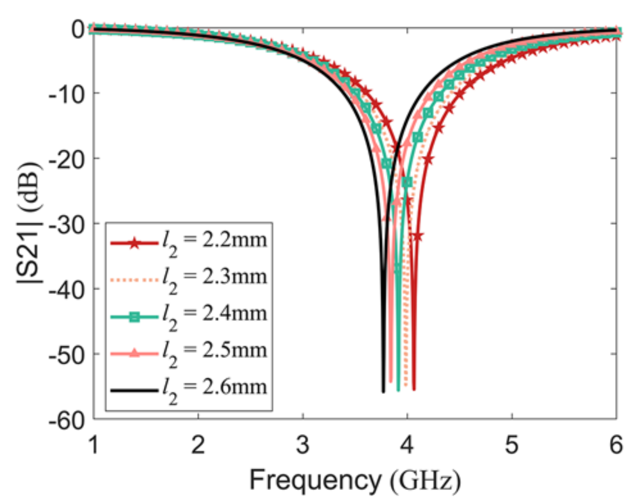

Figure 8. |S21| with variation of *l*2.

Using equations (1)–(3), we obtain the following result of the resonant frequency:

$$f_0 = \frac{1}{\sqrt{L1\,(C1 + C2)}}. \tag{9}$$

The values of inductance and capacitance can be calculated using equations (1)–(3), i.e., L1 = 9.2055 nH, C1 = 0.17765 pF, and C2 = 0.014328 pF. Then, by using Advanced Design System to analyze the equivalent circuit of FSS, the corresponding transmission coefficients are simulated and compared with the CST results, as shown in Fig. 7.

Based on the above equations (1)–(9), the influence of the lumped-element values on the resonant frequency is investigated and described in the following paragraphs.

The resonant frequency is fine-tuned by adjusting the dimensional parameter $l2$, which has an impact on C2. As shown in equation (4), the intermediate variable $g2$ is decreased if $l2$ is increased, which leads to an increase in the capacitance C2 calculated using equation (3). Simultaneously, it is obvious from equation (1) that the inductance L1 increases with $l2$. In Fig. 8, the CST simulation results prove that the change in trend of the resonant frequency with $l2$ is consistent with the above analysis.

In the meantime, the resonant frequency can be effectively regulated by changing the cycle length p. By adjusting the parameter p to alter the intermediate variable $g1$ defined in equation (4), the capacitance C1 is correspondingly changed and determined by equation (2). Figure 9 shows the change in trend of the resonant frequency with cycle length p.

It can also be deduced from equation (1) that the inductance L1 is affected by the strip width $w1$. With the increase of $w1$, the inductance L1 decreases, resulting in an increase in the resonant frequency, as shown in Fig. 10.

Measurement

In order to verify the performance of the proposed FSS, a prototype with 50 × 50 (Fig. 11) units was fabricated and measured

https://doi.org/10.1017/S1759078723001599 Published online by Cambridge University Press

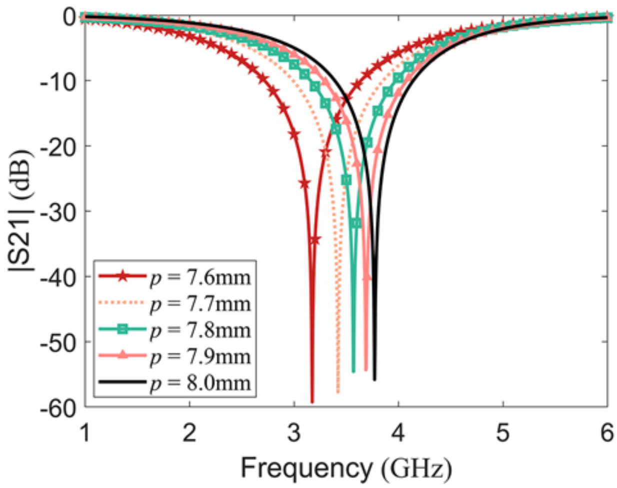

Figure 9. |S21| with variation of *p*.

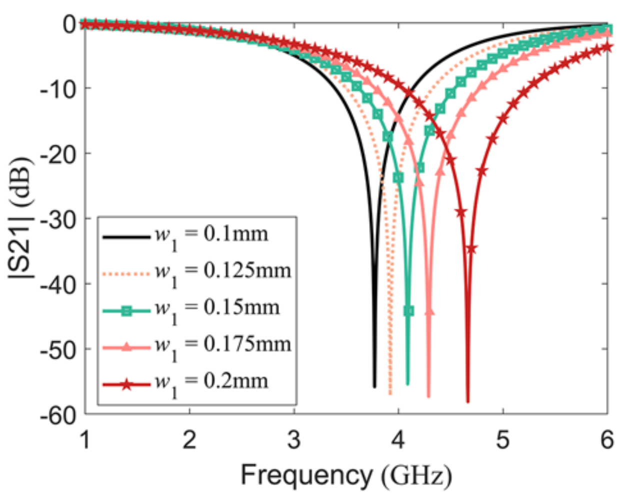

Figure 10. |S21| with variation of *w*1.

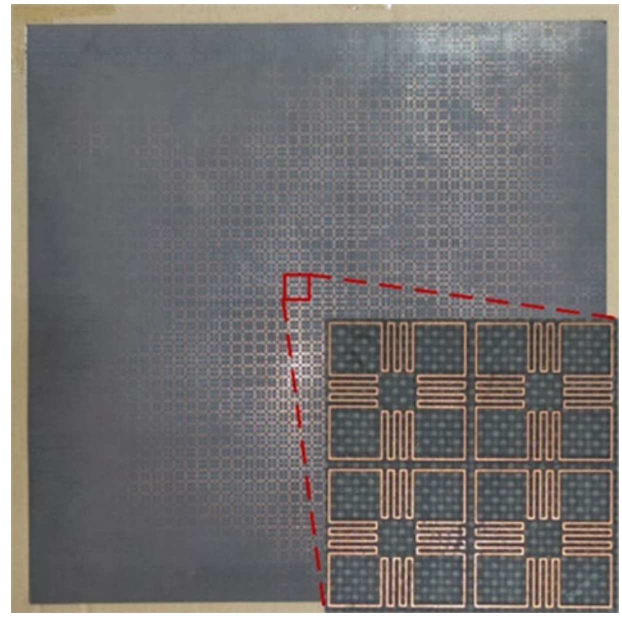

Figure 11. FSS sample. FSS = frequency selective surface.

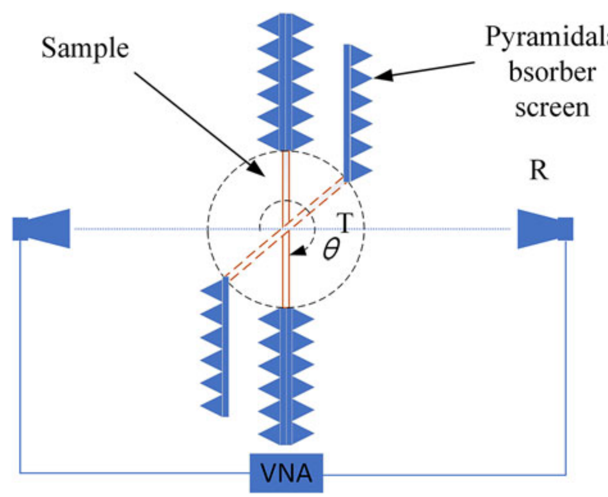

Figure 12. Measurement environment.

by the free-space measurement method. The size of the FSS sample is 400 mm × 400 mm, and the dielectric substrate is F4BK300, which has a relative permittivity of 3, a loss angle tangent of 0.001, and a thickness of 1 mm. As shown in Fig. 12, with the FSS sample mounted on a rotatable table, two standard dual-ridge horn antennas and Agilent 5063A are used for measurements. The maximum aperture of the antenna is 16 mm, and the frequency range is 1–18 GHz. In practical measurements, relevant components are installed according to far-field conditions: the distance between the transmitting antenna and FSS is 0.7 m, the distance between the FSS and the receiving antenna is 1.8 m, and the antenna is 0.8 m above the ground.

Considering that the actual processing thickness of the metal layer is 0.035 mm, the transmission coefficient under different angles of irradiation is re-simulated by CST, as shown in Fig. 13. As the incident angle changes from 0° to 85°, the resonant frequency of the proposed FSS keeps around 3.95 GHz with a maximum deviation of 0.013 GHz (0.33%). Compared with the results in Fig. 5 (where the thickness of the metal layer is not considered), the tendency with angle variation remains unchanged only with a small difference in the resonate frequency.

To evaluate the angular stability of the FSS sample, experiments are implemented according to the setting as described in Figs. 11 and 12. From Fig. 14, it can be found that the measured resonant frequency of the FSS is 3.915 GHz, which is shifted about 45 MHz in comparison with the simulated result in Fig. 13. The tendency for the TE polarization in Fig. 14(a) is that the bandwidth becomes wider as the angle of the incident wave increases, while the opposite tendency is observed for the TM polarization in Fig. 14(b). Evidently, the observed tendency from measurements is in accordance with that by the CST simulation shown in Fig. 13, where the resonant frequency is 3.95 GHz and the angle range is from 0° to 85°.

Figure 15 shows a comparison of the polarization stability to demonstrate the good agreement between simulation and measurement results.

Through the analysis, it is inferred that the shift of resonant frequency between the simulation and the measurement is mainly

https://doi.org/10.1017/S1759078723001599 Published online by Cambridge University Press

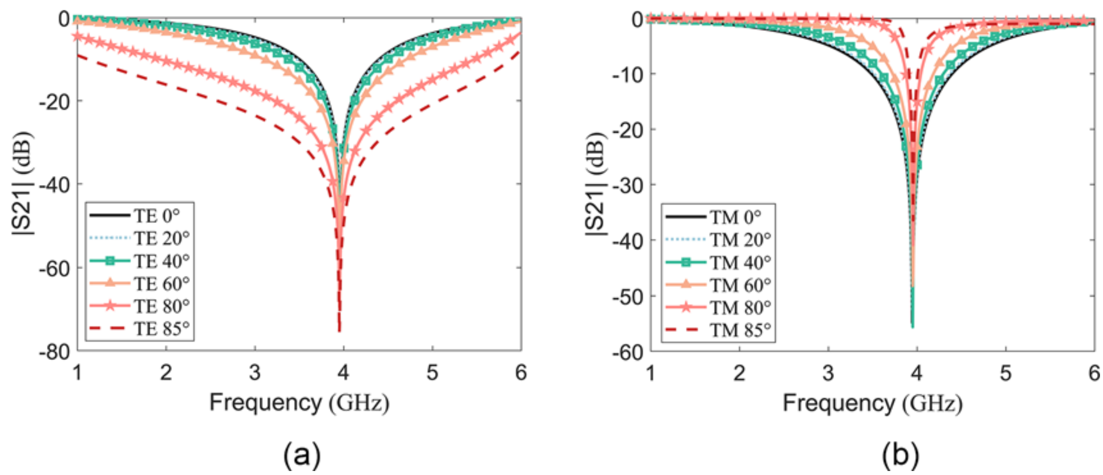

Figure 13. Transmission coefficient with the metal layer thickness of 0.035 mm considered. (a) TE polarization. (b) TM polarization.

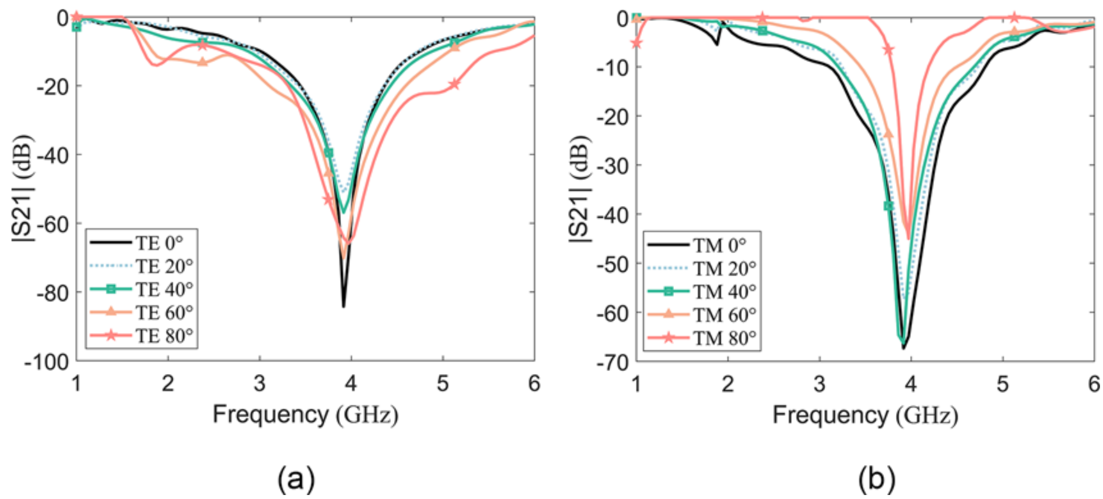

Figure 14. Measured angular performances of FSS sample. (a) TE polarization. (b) TM polarization. FSS = frequency selective surface.

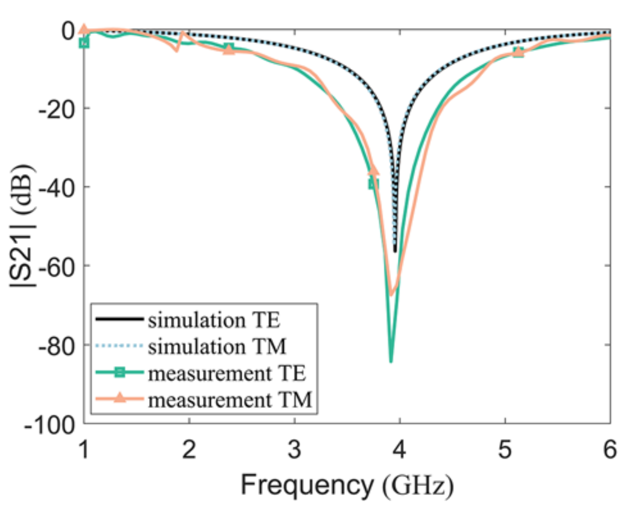

Figure 15. Polarization stability.

caused by the following three reasons: (1) leakage and the bypass are unavoidable during the measurement process; (2) it is difficult to guarantee the flatness of the substrate since the manufactured FSS is just 1 mm thick; and (3) the size of the FSS sample is not large enough to complete the accurate measurement above 80°. In conclusion, the measured results demonstrate a high angular stability of the designed FSS.

In Table 3, the comparison between some recent reported work and this work is made to show the superiority of the designed FSS. It can be seen that the FSS unit structure proposed in this work has the advantages of miniaturization ($0.01\lambda_0$), low profile ($0.0125\lambda_0$), and wide angular stability (up to 85°).

Conclusion

In this paper, a single-layer FSS of simple structure is implemented to achieve angular stability, miniaturization, and low profile through the combination of two different angular stable units. With the help of the software simulation, the FSS structure is designed and optimized, exhibiting a resonant frequency of 3.95 GHz and angular stability up to 85°. To further investigate the mechanism of the FSS, an ECM is developed and the impact of the key dimensional parameters on the frequency response is analyzed. Finally, the prototype was fabricated, and the measurements

https://doi.org/10.1017/S1759078723001599 Published online by Cambridge University Press

Table 3. Comparison with other related FSS designs

Ref.	Type of FSS	Resonant frequency (GHz)	Incident angle	Deviation (GHz)	Unit size	Thickness (mm)
[20]	2D, 1 layer	5.76	0°–85°	0.08	$0.158\lambda_0$	1
[21]	2D, 1 layer	6.29, 8.35	0°–60°	<0.418	$0.168\lambda_0$	1
[22]	2D, 2 layers	3.31	0°–80°	0.06	$0.067\lambda_0$	0.127
[23]	2D, 2 layers	29.6	0°–75°	0.118	$0.355\lambda_0$	0.2
[24]	2.5D	1.6	0°–60°	–	$0.034\lambda_0$	1.6
[25]	2.5D	2.4, 5.5	0°–85°	0.024	$0.52\lambda_0$	1.6
[26]	3D	2.45	0°–80°	0.01	$0.195\lambda_0$	≈ 4.78
This work	2D, 1 layer	3.95	0°–85°	0.013	$0.1\lambda_0$	1

were performed to verify our design. The results show that the proposed FSS structure can achieve angular stability from 0° to 80°, a miniaturization of $0.1\lambda_0$, and a low profile of $0.0125\lambda_0$.

Acknowledgements. This work is supported by the National Natural Science Foundation of China (Nos. 61801357 and 61871458).

Author contributions. Hang Gu designed the structure, performed the research, and analyzed the data. Wei Zhao found the financial support and supervised the project. All authors discussed the experimental method and contributed to the writing.

Competing interests. The authors report that there is no conflict of interest.

References

1. **Mittra R, Chan CH and Cwik T** (1988) Techniques for analyzing frequency selective surfaces-a review. *Proceedings of the IEEE* **76**, 1593–1615.
2. **Bertoni HL and Cheo LHS** (2000) Frequency-selective reflection and transmission by a periodic dielectric layer. *IEEE Transactions on Antennas and Propagation* **37**, 78–83.
3. **Munk B** (2020) *Frequency Selective Surfaces: Theory and Design*. New York: John Wily.
4. **Luo GQ, Hong W, Lai QH, Wu K and Sun LL** (2007) Design and experimental verification of compact frequency-selective surface with quasi-elliptic bandpass response. *IEEE Transactions on Microwave Theory & Techniques* **55**, 2481–2487.
5. **Ghosh S and Srivastava KV** (2015) An equivalent circuit model of FSS-based metamaterial absorber using coupled line theory. *IEEE Antennas and Wireless Propagation Letters* **14**, 511–514.
6. **Ferreira D, Cuiñas I, Caldeirinha RFS and Fernandes TR** (2016) Dual-band single-layer quarter ring frequency selective surface for Wi-Fi applications. *IET Microwaves, Antennas & Propagation* **10**, 435–441.
7. **Liu N, Sheng X, Zhang C and Guo D** (2018) Design of frequency selective surface structure with high angular stability for radome application. *IEEE Antennas and Wireless Propagation Letters* **17**, 138–141.
8. **Guidoum F, Tounsi ML, Vuong TP, Ababou N and Yagoub MCE** (2021) Enhancing 5G antenna performance by using 3D FSS structures. *International Journal of RF and Microwave Computer-Aided Engineering* **31**, e22739.
9. **Yang Y, Li W, Salama KN and Shamim A** (2021) Polarization insensitive and transparent frequency selective surface for dual band GSM shielding. *IEEE Transactions on Antennas and Propagation* **69**, 2779–2789.
10. **Natarajan R, Kanagasabai M, Baisakhiya S, Sivasamy R, Palaniswamy S and Pakkathillam JK** (2013) A compact frequency selective surface with stable response for WLAN applications. *IEEE Antennas and Wireless Propagation Letters* **12**, 718–720.
11. **Ghosh S and Srivastava KV** (2017) An angularly stable dual-band FSS with closely spaced resonances using miniaturized unit cell. *IEEE Microwave and Wireless Components Letters* **27**, 218–220.
12. **Zhao Z, Shi H, Guo J, Li W and Zhang A** (2017) Stopband frequency selective surface with ultra-large angle of incidence. *IEEE Antennas and Wireless Propagation Letters* **16**, 553–556.
13. **Liu N, Sheng X, Zhang C and Fan J** (2018) A design method for synthesizing miniaturized FSS using lumped reactive components. *IEEE Transactions on Electromagnetic Compatibility* **60**, 536–539.
14. **Zhao Z, Li J, Shi H, Chen X and Zhang A** (2018) A low-profile angle-insensitive bandpass frequency-selective surface based on vias. *IEEE Microwave and Wireless Components Letters* **28**, 200–202.
15. **Abidin ZU, Cao Q and Shah G** (2020) Design of a novel miniaturized bandstop frequency selective surface exhibiting polarization insensitivity and enhanced oblique stability. *International Journal of RF and Microwave Computer-Aided Engineering* **30**, e22263.
16. **Li H, Li B and Zhu L** (2021) A generalized synthesis technique for high-order and wideband 3-D frequency-selective structures with hebyshev functions. *IEEE Transactions on Antennas and Propagation* **69**, 3936–3944.
17. **Amin M and Behdad N** (2015) Inductively-coupled miniaturized-element frequency selective surfaces with narrowband, high-order bandpass responses. *IEEE Transactions on Antennas and Propagation* **63**, 4766–4774.
18. **Sung HH, Sowerby KW, Neve MJ and Williamson AG** (2006) A frequency-selective wall for interference reduction in wireless indoor environments. *IEEE Antennas and Propagation Magazine* **48**, 29–37.
19. **Archer MJ** (1985) Invited paper Wave reactance of thin planar strip gratings. *International Journal of Electronics* **58**, 187–230.
20. **Hong T, Xing W, Zhao Q, Gu Y and Gong S** (2018) Single-layer frequency selective surface with angular stability property. *IEEE Antennas and Wireless Propagation Letters* **17**, 547–550.
21. **Li Y, Ren P, Xiang Z, Xu B and Chen R** (2022) Design of dual-stopband FSS with tightly spaced frequency response characteristics. *IEEE Microwave and Wireless Components Letters* **32**, 1011–1014.
22. **Azemi SN, Ghorbani K and Rowe WST** (2015) Angularly stable frequency selective surface with miniaturized unit cell. *IEEE Microwave and Wireless Components Letters* **25**, 454–456.
23. **Chou -H-H and Ke G-J** (2021) Narrow bandpass frequency selective surface with high level of angular stability at Ka-Band. *IEEE Microwave and Wireless Components Letters* **31**, 361–364.
24. **Sampath SS, Sivasamy R and Kumar KJJ** (2019) A novel miniaturized polarization independent band-stop frequency selective surface. *IEEE Transactions on Electromagnetic Compatibility* **61**, 1678–1681.
25. **Wei P-S, Chiu C-N, Chou -C-C and Wu T-L** (2020) Miniaturized dual-band FSS suitable for curved surface application. *IEEE Antennas and Wireless Propagation Letters* **19**, 2265–2269.
26. **Zhu DZ, Werner PL and Werner DH** (2017) Design and optimization of 3-D frequency-selective surfaces based on a multiobjective lazy ant colony optimization algorithm. *IEEE Transactions on Antennas and Propagation* **65**, 7137–7149.

https://doi.org/10.1017/S1759078723001599 Published online by Cambridge University Press

Hang Gu received the B.S. degree in mechanical and electronic engineering from Taiyuan University of Science and Technology, Taiyuan, China, in 2019. He is currently working toward the M.S. degree with the School of Mechanical and Electrical Engineering, Xidian University, Xi'an, China. His research interests include frequency selective surfaces and free-space measurement.

Wei Zhao received the B.S. and M.S. degrees in measurement technology and instrumentation from Xidian University, Xi'an, China, in 2005 and 2008, respectively, and the Ph.D. degree in communication and information system from the Nanjing University of Aeronautics and Astronautics, Nanjing, China, in 2011. He joined Xidian University in 2011. From 2014 to 2015, he was a guest researcher with the National Institute of Standards and Technology, Boulder, CO, USA. He is currently a lecturer at the School of Mechano-Electronic Engineering, Xidian University. His research interests include vector network analyzer (VNA) calibration and uncertainty analysis.

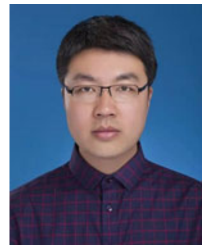

Fan Zhang was born in Shaanxi, China. He received the B.S. degree in measurement technology and instrumentation and the Ph.D. degree in electromagnetic fields and microwave technology from Xidian University, Xi'an, China, in 2005 and 2011, respectively. He is currently a lecturer at the Science and Technology on Antenna and Microwave Laboratory, Xidian University. His current research interests include conformal array antennas and phased array antennas.

Chao Yang received the Ph.D. degree in radiophysics from Xidian University, Xi'an, China, in 2010. He is currently a professor at the School of Science, Xi'an University of Posts & Telecommunications, Xi'an, China. His research interests include electromagnetic wave propagation and scattering in complex environments and random media and optimization techniques in electromagnetic problems.

https://doi.org/10.1017/S1759078723001599 Published online by Cambridge University Press